

[*Electronic Supplementary Information (ESI)*]

## **Dynamic motions of DNA molecules in an array of plasmonic traps**

Jun-Hee Choi,<sup>‡a</sup> Jung-Dae Kim<sup>‡b</sup> and Yong-Gu Lee<sup>\*b</sup>

a Advanced Photonics Research Institute (APRI)

b School of Mechatronics, Gwangju Institute of Science and Technology (GIST)

\* Corresponding author. E-mail: lygu@gist.ac.kr

‡ These authors contributed equally to this work.

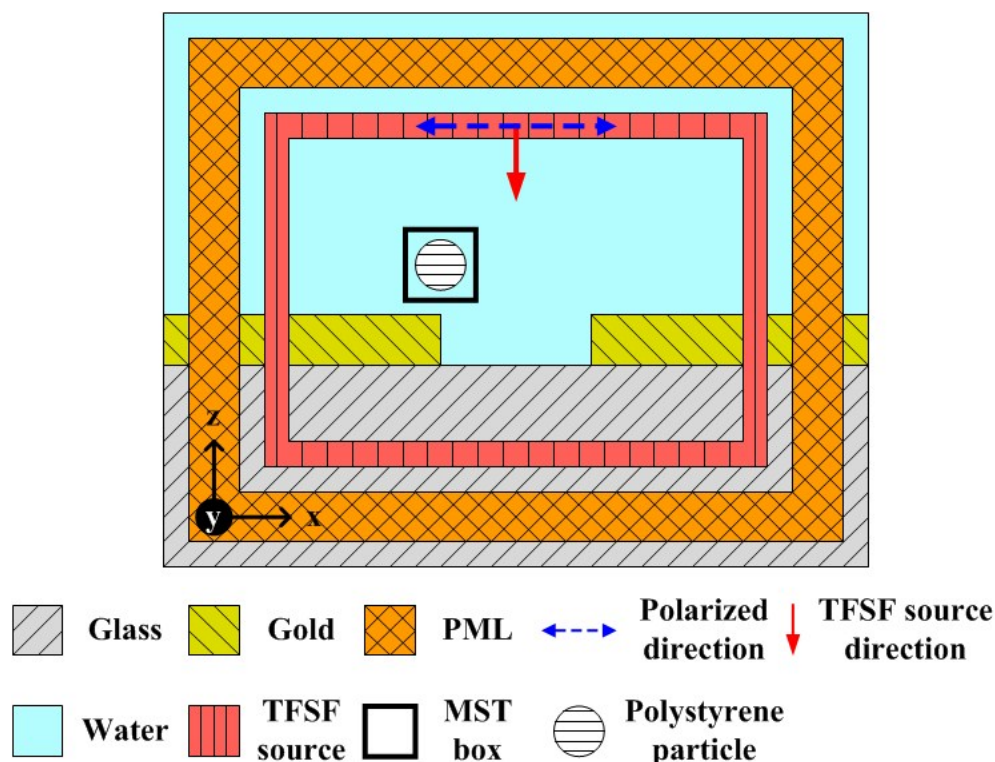


**Fig. S1.** Electromagnetic simulation set up using a gold nanohole to trap a particle which represents the DNA. The diameters of the particle and the nanohole are, 11.13 nm and 400 nm, respectively. Mesh grid distance is 3 nm. Maxwell stress tensor (MST) analysis was used to calculate the trapping force.

Fig. S1 illustrates the modeling used for the simulation. A gold film of 100 nm thickness is deposited on a glass substrate and subsequently etched forming a 400 nm nanohole. A spherical particle is placed at the rim of the nanohole and the electromagnetic field enhancement is computed. Second, we need to select the radius of the spherical particle to substitute the DNA molecule. Approximating the DNA as a small ball having a radius value equal to the radius of gyration,  $r_G$  could be a good choice.<sup>1</sup> However, this would miss the fact that the ball would be very loosely filled with dielectric materials since condensed DNA molecules are mostly empty. Thus, it would be wiser to reduce the diameter of the ball. We have modeled the DNA molecule of 5.4 kbps as a sphere of 11.13 nm radius. This radius is set such that the volume of the sphere equals to the volume of an extremely long cylinder whose length and diameter are 5.4 kbps and 2 nm, respectively.<sup>2</sup> This sphere is placed in the simulation model with a unit laser intensity to compute the field distribution. Subsequently, a box that contains the sphere is used to integrate the MST (Maxwell stress tensor) box to compute the optical force.

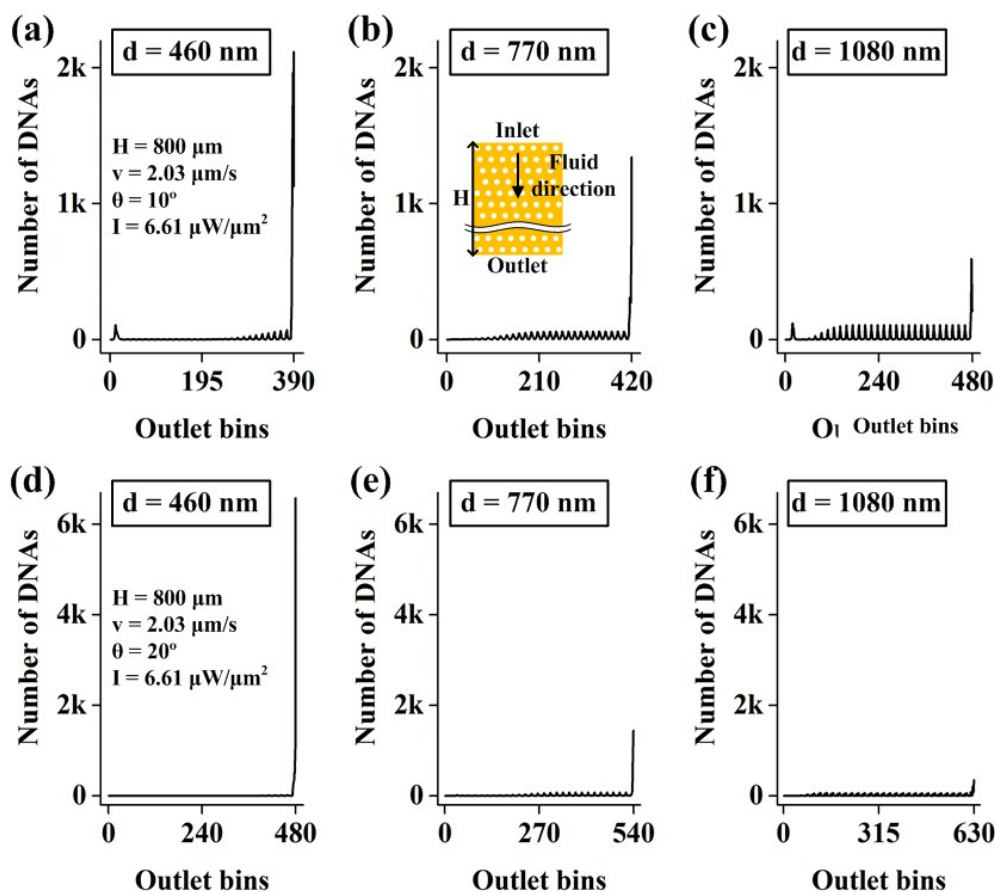


Fig. S2. Accumulation pattern at the chip bottom as a function of distance between two potential wells. Accumulation at the top 10 % of the outlet bins are decreasing as  $d$  increases. (a-c) Accumulation dependence on  $d$  at the fixed conditions of  $H$ ,  $v$ ,  $\theta$ ,  $I$  that are  $800\ \mu\text{m}$ ,  $2.03\ \mu\text{m/s}$ ,  $10^\circ$ ,  $6.61\ \mu\text{W}/\mu\text{m}^2$ , respectively. Each  $d$  is (a)  $460\ \text{nm}$ , (b)  $770\ \text{nm}$ , (c)  $1080\ \text{nm}$ . (d-f) Accumulation dependence on  $d$  at the fixed conditions of  $H$ ,  $v$ ,  $\theta$ ,  $I$  that are  $800\ \mu\text{m}$ ,  $2.03\ \mu\text{m/s}$ ,  $20^\circ$ ,  $6.61\ \mu\text{W}/\mu\text{m}^2$ , respectively. Each  $d$  is (d)  $460\ \text{nm}$ , (e)  $770\ \text{nm}$ , (f)  $1080\ \text{nm}$ .

In Fig. S2, we provide another set of results by varying the  $d$ , the center to center distance between the nanoholes, with all other conditions fixed. Fig. S2a-c show the accumulation graph with  $v$  and  $\theta$  fixed at  $2.03\ \mu\text{m/s}$  and  $10^\circ$ , respectively. From observing Fig. S2a-c, we can see that the chains accumulated at the rightmost bins decrease as  $d$  increases. If we increase  $\theta$  to  $20^\circ$ , the decreasing rate increases as shown in Fig. S2d-f. The stronger accumulation to the rightmost bin happens for smaller  $d$  because the chains can safely jump to the next potential well without getting pushed by the fluid at the gap between the two potential wells.

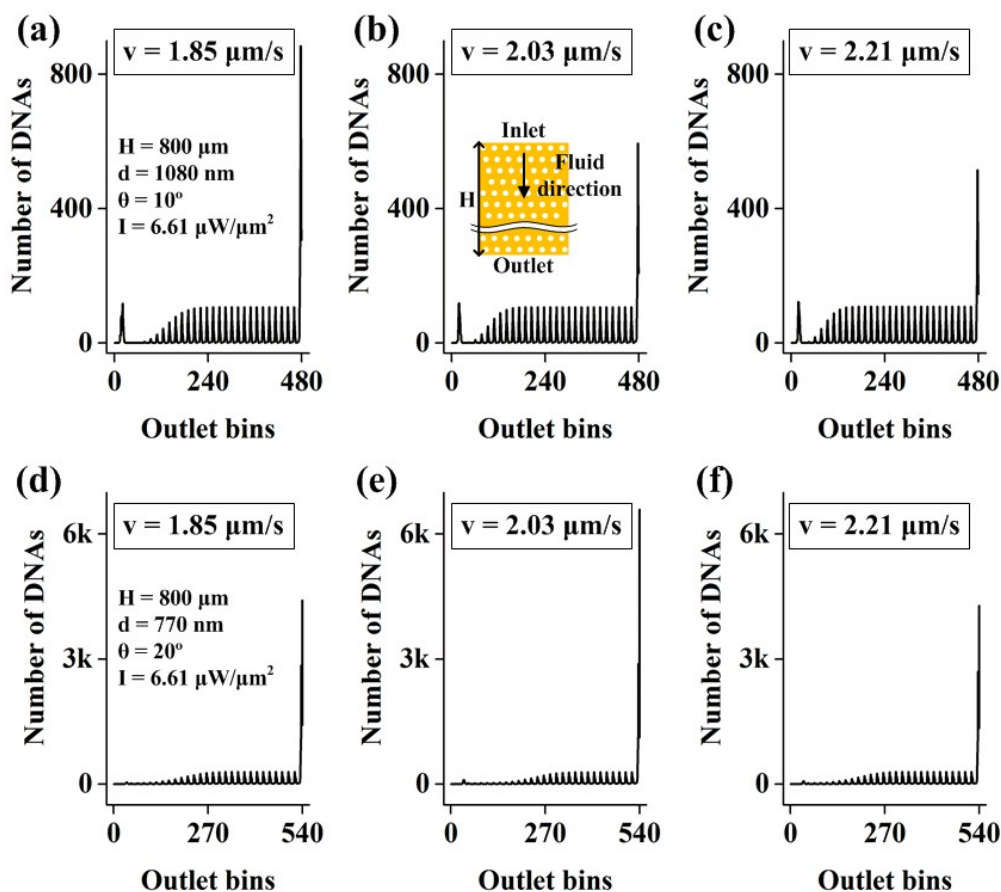


Fig. S3 Accumulation pattern at the chip bottom as a function of the fluid velocity. (a-c) Accumulation dependence on  $v$  at the fixed conditions of  $H$ ,  $d$ ,  $\theta$ ,  $I$  that are  $800 \mu\text{m}$ ,  $1080 \text{ nm}$ ,  $10^\circ$ ,  $6.61 \mu\text{W}/\mu\text{m}^2$ , respectively. Each  $v$  is (a)  $1.85 \mu\text{m/s}$ , (b)  $2.03 \mu\text{m/s}$ , (c)  $2.21 \mu\text{m/s}$ . (d-f) Accumulation dependence on  $v$  at the fixed conditions of  $H$ ,  $d$ ,  $\theta$ ,  $I$  that are  $800 \mu\text{m}$ ,  $770 \text{ nm}$ ,  $20^\circ$ ,  $6.61 \mu\text{W}/\mu\text{m}^2$ , respectively. Each  $v$  is (d)  $460 \text{ nm}$ , (e)  $770 \text{ nm}$ , (f)  $1080 \text{ nm}$

Fig. S3 gives the effect of changing the fluid velocity,  $v$ . In Fig S3a-c,  $d$  and  $\theta$  are fixed at  $1080 \text{ nm}$  and  $10^\circ$ , respectively. We can see the peak accumulation at the rightmost bin happens when the fluid velocity is  $1.85 \mu\text{m/s}$ , and declines as the velocity increases. Note similar trend cannot be observed for different  $d$  and  $\theta$ ,  $770 \text{ nm}$  and  $20^\circ$ , respectively. Observation of the Fig. S3d-f tells us that the peak accumulation to the right happens at the middle fluid velocity,  $2.03 \mu\text{m/s}$ . For this, we can conclude that there is a local maxima somewhere near the middle fluid velocity.

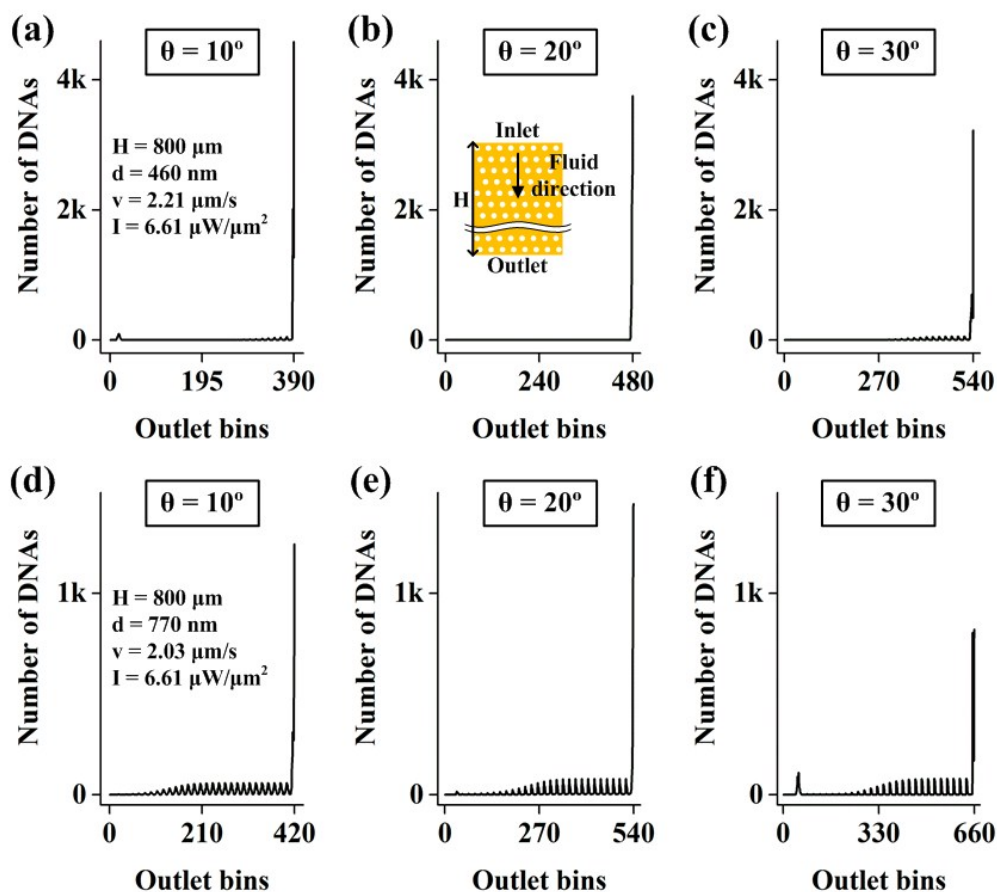


Fig. S4 Accumulation pattern at the chip bottom as a function of the potential wells inclination angle,  $\theta$ . (a-c) Accumulation dependence on  $\theta$  at the fixed conditions of  $H$ ,  $d$ ,  $v$ ,  $I$  that are  $800\ \mu\text{m}$ ,  $460\ \text{nm}$ ,  $2.21\ \mu\text{m/s}$ ,  $6.61\ \mu\text{W}/\mu\text{m}^2$ , respectively. Each  $\theta$  is (a)  $10^\circ$ , (b)  $20^\circ$ , (c)  $30^\circ$ . (d-f) Accumulation dependence on  $\theta$  at the fixed conditions of  $H$ ,  $d$ ,  $v$ ,  $I$  that are  $800\ \mu\text{m}$ ,  $770\ \text{nm}$ ,  $2.03\ \mu\text{m/s}$ ,  $6.61\ \mu\text{W}/\mu\text{m}^2$ , respectively. Each  $\theta$  is (d)  $10^\circ$ , (e)  $20^\circ$ , (f)  $30^\circ$

Fig. S4 is obtained by fixing all other variables except the angle,  $\theta$ . Fig. S4a-c are obtained by setting  $d$  and  $v$  to  $460\ \text{nm}$  and  $2.21\ \mu\text{m/s}$ , respectively. The angle formed by the potential wells,  $\theta$  is the key driving factor. From observing the plot, we can see that the peak accumulation to the right happens when  $\theta$  is  $10^\circ$  and accumulation diminishes for the increased  $\theta$ . However for different,  $d$  and  $v$ ,  $770\ \text{nm}$  and  $2.03\ \mu\text{m/s}$ , respectively. Fig. S4d-f show the peak happens when  $\theta$  is  $20^\circ$ .

1. J.-D. Kim and Y.-G. Lee, *Biomed. Opt. Express*, 2014, **5**, 2471-2480.
2. B. Boudaïffa, P. Cloutier, D. Hunting, M. A. Huels and L. Sanche, *Science*, 2000, **287**, 1658-1660.